Magnetic origin of phase stability in cubic γ-MoN

Xu Zheng,[1,2,a)] Huili Wang,[1,3,4,a)] Xiaohui Yu,[1,b)] Junsheng Feng,[5] Xi Shen,[1] Sijia Zhang,[1] Rong Yang,[6] Xuefeng Zhou,[2] Yue Xu,[7] Richeng Yu,[1] Hongjun Xiang,[5] Zhenpeng Hu,[4] Changqing Jin,[1,b)] Ruifeng Zhang,[8] Suhuai Wei,[9] Jiantao Han,[7] Yusheng Zhao,[10] Hui Li,[3,b)] and Shanmin Wang[10,b)]

[1]*Beijing National Laboratory for Condensed Matter Physics, and Institute of Physics, Chinese Academy of Sciences, Beijing 100190, China*
[2]*School of Physical Sciences, University of Chinese Academy of Sciences, Beijing 100049, China*
[3]*Beijing Advanced Innovation Center for Soft Matter Science and Engineering, Beijing University of Chemical Technology, Beijing 100029, China*
[4]*Department of Physics, Nankai University, Tianjin 300072, China*
[5]*Department of Physics, Fudan University, Shanghai 200433, China*
[6]*Institute of Mechanics, Chinese Academy of Sciences, Beijing 100190, China*
[7]*School of Materials Science and Engineering, Huazhong University of Science and Technology, Wuhan 430074, China*
[8]*School of Materials Science and Engineering, Beihang University, Beijing 100191, China*
[9]*Beijing Computational Science Research Center, Beijing 100193, China*
[10]*Department of Physics, Southern University of Science and Technology, Shenzhen 518055, China*

(Received 16 July 2018; accepted 25 October 2018; published online 26 November 2018)

Among transition-metal nitrides, the mononitride γ-MoN with a rock-salt structure has drawn particular attention because it has been predicted to possess excellent mechanical and electronic properties, especially the high superconducting temperature around 30 K. However, synthesis of bulk γ-MoN_x with the nitrogen concentration, x, more than 0.5 is still challenging, leading to contradictions on its phase stability and properties. In this work, we formulated a high-pressure synthesis reaction for the formation of single-crystal γ-MoN_x with a remarkably high nitrogen concentration value of $x \approx 0.67$. This nitride possesses a high asymptotic hardness of ~24 GPa, which is so far the second hardest among metal nitrides. Impressively, the expected superconductivity is absent in the as-synthesized product. We further performed density functional theory calculations to clarify the structural stability and the absence of superconductivity in stoichiometric γ-MoN. We find that the ground state of γ-MoN is theoretically explored to be a Mott insulator with an antiferromagnetic phase, while a paramagnetic configuration is adopted at the ambient conditions. Such magnetic properties would explain the structural stability and the absence of superconductivity in the as-synthesized γ-MoN_x with a high nitrogen concentration. *Published by AIP Publishing.*
https://doi.org/10.1063/1.5048540

Refractory transition-metal (TM) nitrides have attracted particular scientific and industrial interest because of their high hardness, high melting points, and even superconductivity with considerably high critical temperatures (T_c).[1–3] However, despite intensive studies, some fundamental underlying physics of TM nitrides, especially the relationship between phase stability and the electronic structure, remains poorly understood. Most early TM nitrides favor to crystallize into a mononitride with a rock-salt structure, while the mononitrides with heavier TM elements prefer to adopt the zinc-blend (e.g., FeN and CoN) and hexagonal (e.g., δ-WN and δ-MoN) structure modifications.[4–7] Such structural variations lead to the diversity of their physical and chemical properties. For example, the TM nitrides with the rocksalt structure (B1) often demonstrate a relatively higher T_c than that of the hexagonal phase (e.g., NbN, ZrN, and HfN).[8,9] The known highest T_c of TM nitrides is ~16 K as found in cubic NbN.[10] Impressively, based on the Gaspari-Gyorffy approach,[11,12] it has been proposed that the cubic γ-MoN could possess superconductivity with an even higher transition temperature of ~29 K,[13] making this compound a fantastic material.

Over the past few decades, attempts to experimentally validate this prediction in γ-MoN have been unsuccessful mainly because the preparation of high-quality γ-MoN with the composition close to stoichiometry is still challenging.[14–16] Most previously reported products are poorly crystallized and non-stoichiometric in the form of thin films synthesized through traditional reaction routes.[15,17–19] As a result, the stability of this compound is still an unsettled problem, according to a number of recent calculations.[20] Both the calculated negative elastic constant C_{44} and the imaginary frequency in phonon spectra indicate that the structure of γ-MoN_x is metastable and would spontaneously transform into the hexagonal lattice.[20–24] A series of theoretical works suggests that high pressure would be favorable for the formation of γ-MoN_x with a high nitrogen concentration.[25,26] Recently, synthesis of bulk γ-$MoN_{0.54}$ has been reported in Ref. 14, showing a record value of the nitrogen concentration and a large lattice parameter of 4.188 Å. In addition, the obtained T_c for bulk γ-$MoN_{0.54}$ is 9.5 K, which

[a)]X. Zheng and H. Wang contributed equally to this work.
[b)]Authors to whom correspondence should be addressed: yuxh@iphy.ac.cn; jin@iphy.ac.cn; hli@buct.edu.cn; and wangsm@sustc.edu.cn.

is much higher than that in the previous report (i.e., 5.5 K),[15,16] indicating the sensitivity of its superconductivity to nitrogen deficiency. To date, single-crystal γ-MoN_x has rarely been reported, in particular with a high nitrogen concentration. Therefore, more experimental efforts are needed to address the afore-mentioned issues.

Using a special high-pressure (P) reaction route, we have recently synthesized a series of interesting TM nitrides in W-N,[27] Mo-N,[28–30] Cr-N,[31,32] and V-N systems,[33] including synthesis of γ-MoN_x single crystals.[30] In this work, we further have investigated this nitride with both experiments and first-principles calculations with a focus on its phase stability from the perspective of magnetism.

The single-crystal γ-MoN_x samples were synthesized using the recently formulated ion-exchange reaction at high pressure, referring to Refs. 30 and 33 for more experimental details. Single-crystal and powder X-ray Diffraction measurements were employed to identify the phase of as-grown crystals, equipped with Mo and copper targets, respectively. The chemical composition of γ-MoN_x was determined by carrying out both energy-dispersive X-ray spectroscopy (EDX) and an electron probe micro-analyzer (EPMA, SHIMADZU), using stoichiometric hexagonal δ-MoN single crystal as a reference material.[30] Experimental details of the EPMA of TM nitride can be referred to Ref. 34. Raman spectroscopy was used to study the possible nitrogen deficiency as mentioned in Ref. 14. The aberration-corrected scanning transmission electron microscopy (STEM, JEOL ARM200F) measurement was performed to study the material at the atomic level. Annular bright-field (ABF) and high-angle annular dark-field (HAADF) images were acquired at angles of 11.5–23.0 and 90–370 mrad, respectively. The low-temperature electrical resistivity was conducted using a four-probe method. We used a dual-beam Strata DB 235 focused ion beam (FIB)/scanning electron microscopy (SEM) system to prepare four electrical contact pads by a Pt source on the (111) crystallographic plane of selected single crystals. The nano-indentation hardness measurements were performed at the applied loads of 5, 10, 15, and 20 mN using a Berkovich indenter and a continuous stiffness measurement (CSM) mode with a strain rate of 0.05 s^{-1}. The loading time and holding time were 30 s and 10 s, respectively. The reduced elastic modulus (or combined modulus) was derived using the well-known Oliver-Pharr method.[35]

Density functional theory (DFT) calculations were carried out using the Vienna *ab initio* simulation package (VASP).[36] The Perdew-Burke-Ernzerhof (PBE) function was employed combined with the projector-augmented wave (PAW) pseudopotentials,[37,38] as well as plane-wave basis sets with an energy cutoff at 520 eV. The Monkhorst–Pack scheme of k-point sampling was used on grids of $11 \times 11 \times 11$ for the cubic and orthogonal 8-atom MoN unit cell and $5 \times 7 \times 7$ for the 48-atom supercell. In the DFT+U correction, the U–J value (4.38 eV) for the Mo 4d-orbitals was used from the previous benchmark of formation energies for Mo oxides.[39] All the structures were optimized until the maximum force on each atom is less than 0.01 eV/Å.

The crystal structure of the high-P synthesized sample is determined using transmission electron microscopy (TEM) and single-crystal x-ray diffraction (XRD). As displayed in Fig. 1(a), its crystal structure can readily be indexed by a cubic symmetry with a space group of $Fm\bar{3}m$ (No. 255), and the determined lattice parameter is $a = 4.2$ Å along the [011] zone-axis. Figure 1(b) shows the well-defined atomic fringe patterns of Mo atoms, confirming the high quality of the as-prepared sample. Although the nitrogen atoms can be observed in Fig. 1(c), it is hard to determine the nitrogen deficiency, owing to the low sensitivity of nitrogen to the electron microscopy probe. However, using intensity based on line scanning along a certain crystallographic plan, the nitrogen disorder and deficiency are clearly explored, which suggests sub-stoichiometry of the sample (see Fig. S1). Besides, the rock-salt structure as shown in Fig. 1(d) can further be confirmed by single-crystal and powder XRDs. The calculated lattice parameter is $a = 4.1952(12)$ Å, which agrees well with the obtained value by TEM. It is noted that such-determined lattice parameter is close to that of stoichiometric γ-MoN (i.e., ~4.21 Å) in the form of the thin film as claimed by Inumaru *et al.*,[15] inferring a high-nitrogen concentration, because the lattice parameter of nitride is very sensitive to the x value in TMN_x. However, complicating the matter further is that the lattice parameter of our sample is just slightly greater than that of high-P synthesized γ-$MoN_{0.54}$ (i.e., 4.188 Å) by Bailey and McMillan,[14] indicating a sub-stoichiometric composition in the our sample. In fact, XRD refinement also shows that the x value in our sample should be in the range of 0.6–0.8 (Fig. S2).

To determine the chemical composition of this nitride, we performed both EDX and EPMA measurements using hexagonal single-crystal δ-MoN as a standard. Because of the remarkable difference in sensitivity to EDX between Mo and N, the obtained x value is around 0.53 in the EDX method (Fig. S3 and Table S1). In contrast, the EPMA method is often more accurate and has extensively been used for the

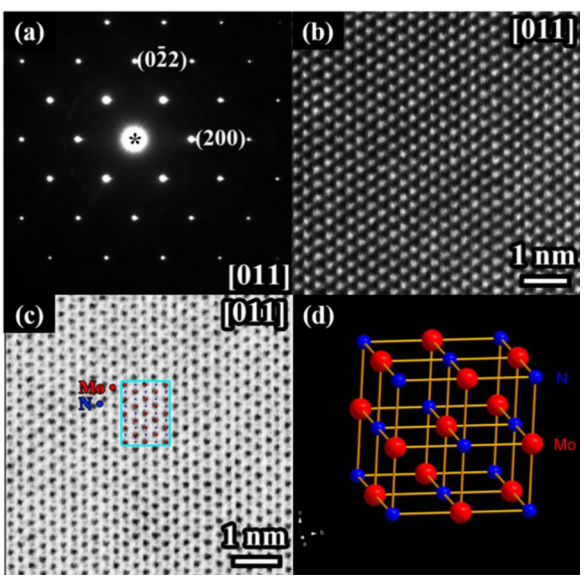

FIG. 1. Structure and the lattice parameter of cubic MoN_x. (a) The selected area electron diffraction (SAED) pattern. (b) The high angle annular dark field (HAADF) images along the [011] zone-axis. (c) The annular bright field (ABF) image along the [011] zone-axis. (d) Ball and stick model. The small blue balls represent the N atoms, and the big red balls represent the Mo atoms.

study of TMN_x.[14,34] Accordingly, the final composition is γ-$MoN_{0.67}$ (i.e., $x \approx 0.67$) (Table S2), which is consistent with the lattice parameter determination, compared with the case of γ-$MoN_{0.54}$.[14] It is noted that we also observed a series of Raman signals from the $MoN_{0.67}$ crystal (Fig. S4), which is closely associated with nitrogen deficiency as reported in Refs. 14 and 40. In addition, probably because the fraction of oxygen in our sample is too low, we did not obtain the enough EPMA signal for oxygen to analyze its contribution. Evidently, synthesis of single-crystal γ-MoN_x with a high nitrogen concentration x $\approx$ 0.67 in this work suggests that the formation of nitride is thermodynamically favorable at high pressure.

The hardness and modulus of the as-prepared single-crystal sample are determined based on the nano-indentation tests performed on the (111) surface. As shown in Fig. 2(a), the modulus and hardness increase gradually with the indented depth of diamond tip into the sample, followed by approaching asymptotic values of 358 GPa and 24 GPa, respectively, at the indented depth of 70 nm. At this threshold depth, the shear deformation starts to be predominant under indentation rather than the elastic deformation. The such-measured modulus and hardness of γ-$MoN_{0.67}$ are comparable to those of Si_3N_4, one of the most widely used hard materials.[41,42]

As shown in Fig. 2(b), we preformed low-temperature resistivity measurement to study superconductivity of single-crystal γ-$MoN_{0.67}$. Remarkably, the measured resistivity decreases as the temperature is lowered, indicating a metallic behavior as plotted in Fig. 2(b). However, the highly expected superconductivity transition is not observed in this single crystal sample with temperature down to 2 K. In fact, the suppression of superconductivity has previously been studied in γ-MoN_x thin films with the increasing high nitrogen concentration as manifested by the increasing lattice parameter.[15] As discussed below, a strong spin fluctuation is associated with stoichiometric γ-MoN, which destroys electron pairing to preclude the formation of superconductivity. In contrast, the lattice defects (i.e., nitrogen deficiency) would suppress the spin fluctuation, leading to superconductivity. From this point of view, our previously observed superconductivity ($T_c \approx 5$ K) in γ-MoN_x (see Ref. 30) should correspond to a smaller x value. Moreover, it is worthwhile to mention that the derived residual resistivity ratio, $\rho_{300\ K}/\rho_0$, is 1.9 [see Fig. 2(b)], which is indicative of magnetically induced scattering of conducting electrons.

To further understand the phase stability and magnetic properties of this material, we carried out the first-principles calculations to evaluate the stabilities of stoichiometric γ-MoN. Due to the crucial role of the on-site Coulomb interaction of localized electrons in transition metal oxides and nitrites, the generalized gradient approximation combined with Hubbard U correction (GGA+U) was employed for treating the Mo 4d-orbitals.[43–45] We compared the energies of various magnetic configurations, including the ferromagnetic (FM) phase and the $Mo_{\uparrow 0.5}Mo_{\downarrow 0.5}N$ antiferromagnetic (AFM) phase with the same magnetic order of CrN [Figs. 3(a)–3(b)],[46] as well as the non-magnetic (NM) phase. As shown in Fig. 3(b), the total energy of stoichiometric MoN for the AFM state (–15.36 eV) is lower than that for both the FM (–14.90 eV) and NM states (–13.96 eV) at the optimized lattices, indicating that the ground state of γ-MoN adopts an AFM state. Furthermore, the binding energy of γ-MoN demonstrates that it is a stable phase against decomposition into $Mo_2N + N_2$. On the other hand, in the conventional PBE calculation without Hubbard U potential, the NM state is the ground state, as shown in Fig. S5.

The kinetic stability of the AFM phase is further confirmed, since no observable imaginary frequency is found in the phonon spectrum [Fig. 3(c)]. The FM state is also found

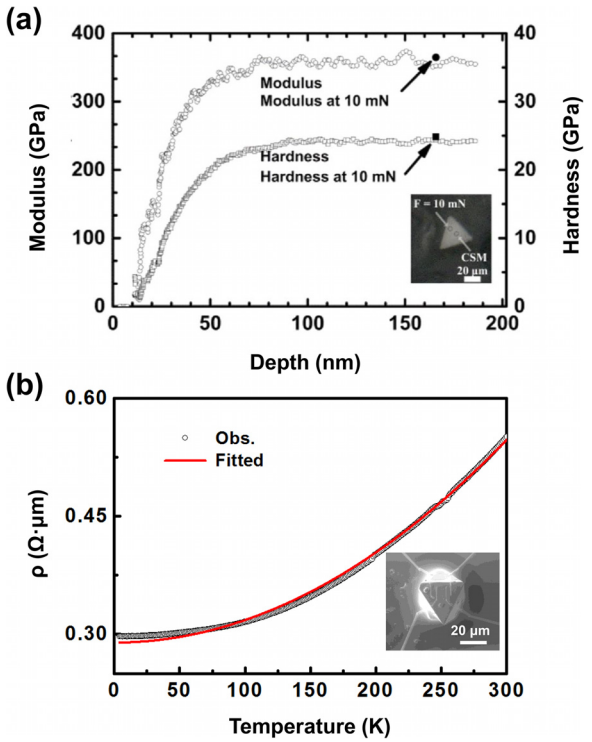

FIG. 2. Electron transport and mechanical properties of single-crystal γ-$MoN_{0.67}$. (a) Nano-indentation tests on the (111) crystallographic plane. (b) The measured electrical resistivity as a function of temperature down to 2 K (black circles). For the residual resistivity, $\rho_0 = 0.289\ \Omega{\cdot}\mu m$, is extrapolated from a fit of the data to $\rho = \rho_0 + AT^2$ (red lines), where T and A are the temperature and constant, respectively.

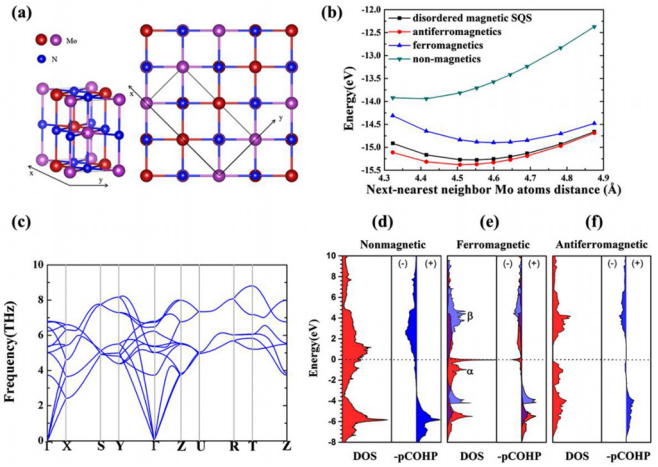

FIG. 3. (a) and (b) Perspective and top view of the MoN orthorhombic cell with antiferromagnetic spin moments. The red and purple balls stand for two right about magnetic moments of Mo atoms. The blue balls stand for N atoms. (b) Energy of MoN unitcell as a function of Mo atom's next-nearest neighbor distance. (c) Phonon dispersions for the AFM phase. (d)–(f) DOS and –pCOHP plots of the cubic nonmagnetic and ferromagnetic structure and of the orthorhombic structure.

to be kinetically stable with only a tiny imaginary frequency of –0.02 THz in the transverse acoustic phonon branch around the Γ-point [Fig. S6(b)]. The kinetic instability of the NM phase is also confirmed by a large negative frequency of –10 THz in its phonon spectra using both the GGA+U and the conventional GGA calculations [Fig. S6(a)]. It is noted that some kinetically unstable structures can be stabilized at high temperature. For example, the imaginary frequency of the ε-Pu phase can be eliminated by its phonon entropy at 1500 K.[47] However, extremely high temperature may be needed to eliminate the imaginary frequency of –10 THz, while all the experimental measurements were performed at ambient conditions. Therefore, the temperature effect for stabilizing the NM phase can be excluded. According to the first principles calculations, the AFM state of γ-MoN processes both thermodynamic and dynamic stabilities.

Due to the spin polarization, the calculated lattice parameters of magnetic states (e.g., 4.6 Å for the FM state and 4.5 Å for the AFM state) are larger than those of the NM state (4.34 Å), which is greater than those of γ-$MoN_{0.67}$ (∼4.2 Å), although the NM state is both thermodynamically and kinetically unstable. Similar overestimation of the lattice parameters was also reported in previous GGA+U calculations.[48] It is further noted that the anisotropic spin distribution leads to slightly deformation of the lattice for AFM γ-MoN. According to our calculation, a contraction of ∼3.5° for the inter-axial angle α is found, and the Mo-Mo distance in the *xy* plane (4.528 Å) is 0.5% larger than that along the z axis (4.48 Å) in the AFM configuration.

The calculated band structure demonstrates that the AFM phase of γ-MoN is a Mott insulator with an energy gap of ∼1.0 eV [Fig. S7(b)], while the FM state is metallic [Fig. S7(a)]. Both phases have close local magnetic moments for each Mo atom (AFM: 2.67 μB; FM: 2.86 μB). To gain deeper insight into orbital origins of magnetism, the crystal orbital Hamilton population (COHP) analysis was performed using the LOBSTER package.[49,50] The –pCOHP value as a function of energy can demonstrate details of Mo-N bonding information, where positive and negative values stand for bonding and antibonding states, respectively. As exhibited in Fig. 3(d), the Fermi level located in the antibonding region implies that structure distortion is required for the NM state. Similarly, the Fermi level falls in the antibonding region for only electrons of one spin orientation [Fig. 3(e)], implying that the FM state has higher stability than the NM state, but still lower than the AFM state. The Fermi level of the AFM state is located in the non-bonding region [Fig. 3(f)], where the diminished antibonding states greatly stabilize this configuration.

Although the GGA+U calculation demonstrates that the AFM state is the global minimum, the transportation measurement displays that γ-MoN has a paramagnetic (PM) state with metallic conductivity at the ambient conditions. The ∼0.5% deformation from the cubic structure due to anisotropic magnetic distribution is not noticed in the X-ray diffraction, either. To probe the existence of the PM state, the Special Quasi-random Structure (SQS) method was employed to mimic the disordered local magnetic moments on the cubic lattice.[51] As shown in Fig. 3(b), the SQS-PM state has very close binding energy (∼0.1 eV) and identical lattice parameter to the AFM structure, indicating the extremely easy transition between the AFM and PM states.

To accurately evaluate the Néel temperature (T_N) for magnetism phase transition, we further performed the Monte Carlo (MC) simulation using the extracted spin exchange parameters. To get the Heisenberg exchange parameters J within the first-principles framework, we carried out GGA+U calculations using the four-state mapping approach.[52,53] Based on the calculated spin exchange parameters, the nearest neighbor exchange interaction $J_1 = 0.0408497725$ eV, and the next nearest neighbor exchange interaction $J_2 = 0.0150670150$ eV. The first-principles calculations with parallel temper Monte-Carlo (PTMC) simulation indicate that the T_N is around 162 K, as shown by the specific heat in Fig. S8. In addition, the DOS of the SQS model (Fig. S9) also exhibits a metallic electronic structure for the PM state, in agreement with the experimental measurement. As a result, it is believed that the long-range order of local magnetic moments of the AFM ground state is easily interrupted by small perturbation, such as thermal fluctuation. It should be further mentioned that the conductance measurement shows that the whole sample is metallic even at very low temperature, indicating that the magnetic order is also quite sensitive to structure distortion such as defects, domain boundaries, and surfaces of the small sized crystallites. Therefore, local paramagnetic configurations may always exist in γ-MoN, leading to low macroscopic metallicity.

We have investigated the crystal and electronic structures of single-crystal γ-$MoN_x$with a high nitrogen concentration $x = 0.67$, using a high-pressure approach. This nitride is a hard material with the second highest hardness of 24 GPa among transition-metal nitrides. The highly expected superconductivity is absent in γ-MoN_x because of coexisting strong spin fluctuation in this nitride with a high nitrogen concentration. Further, first-principles calculations suggest that γ-MoN_x with low nitrogen deficiency adopts an antiferromagnetic ground state, which is closely associated with the absence of superconductivity in this material. At ambient conditions, the nitride has a paramagnetic configuration. Our finding solves the long-standing debate in the stability of γ-MoN_x and gains deeper understanding of properties for transition metal nitrides.

See supplementary material for more calculations including binding energies based on the conventional PBE methods and also for phonon spectra, electronic band structures for the ferromagnetic and antiferromagnetic states, density of states for the Special Quasi-Random Structure model, specific heat calculations, and the refined lattice parameter for the nitride using single-crystal XRD.

This work was partially supported by the National Key R&D Program of China (2016YFA0401503) and the National Science Foundation of China (11575288, 51471018, 21773005, and 51402350). This work was partially supported by the Shenzhen Peacock Plan (No. KQTD2016053019134356), the Guangdong Innova-tive & Entrepreneurial Research Team Program (No. 2016ZT06C279), and the Shenzhen Development and Reform Commission Foundation for Novel Nano-Material Sciences. This work was also supported by BUCT Fund for Disciplines Construction (Project No. XK1702).

The authors declare that they have no competing financial interests.

[1]Z. G. Wu, X. J. Chen, V. V. Struzhkin, and R. E. Cohen, Phys. Rev. B **71**, 214103 (2005).
[2]S. H. Jhi, J. Ihm, S. G. Louie, and M. L. Cohen, Nature **399**, 132 (1999).
[3]A. Friedrich, B. Winkler, L. Bayarjargal, W. Morgenroth, E. A. Juarez-Arellano, V. Milman, K. Refson, M. Kunz, and K. Chen, Phys. Rev. Lett. **105**, 085504 (2010).
[4]Y. Zhang, N. Haberkorn, F. Ronning, H. Wang, N. A. Mara, M. Zhuo, L. Chen, J. H. Lee, K. J. Blackmore, E. Bauer *et al.*, J. Am. Chem. Soc. **133**, 20735 (2011).
[5]C. Wang, Q. Tao, S. Dong, X. Wang, and P. Zhu, Inorg. Chem. **56**, 3970 (2017).
[6]D. L. Peng, T. Hihara, and K. Sumiyama, J. Alloys Compd. **377**, 207 (2004).
[7]P. Lukashev and W. R. L. Lambrecht, Phys. Rev. B **70**, 245205 (2004).
[8]E. G. Maksimov, S. Q. Wang, M. V. Magnitskaya, and S. V. Ebert, JETP Lett. **87**, 437 (2008).
[9]X. Y. Li, G. B. Li, F. J. Wang, T. C. Ma, D. Z. Yang, and Y. C. Zhu, Vacuum **43**, 653 (1992).
[10]I. Rudnev, S. Antonenko, D. V. Shantsev, T. H. Johansen, and A. Primenko, Magneto-Optical Imaging **142**, 229 (2004).
[11]H. Rietschel, Z. Phys. B-Condens. Matter **30**, 271 (1978).
[12]W. E. Pickett, B. M. Klein, and D. A. Papaconstantopoulos, Physica B **107**, 667 (1981).
[13]D. A. Papaconstantopoulos, W. E. Pickett, B. M. Klein, and L. L. Boyer, Nature **308**, 494 (1984).
[14]E. Bailey and P. F. McMillan, J. Mater. Chem. **20**, 4176 (2010).
[15]K. Inumaru, K. Baba, and S. Yamanaka, Phys. Rev. B **73**, 052504 (2006).
[16]T. Kawashima, E. Takayama-Muromachi, and P. F. McMillan, Phys. C **460-462**, 651 (2007).
[17]N. Savvides, J. Appl. Phys. **62**, 600 (1987).
[18]K. Saito and Y. Asada, J. Phys. F: Met. Phys. **17**, 2273 (1987).
[19]G. Linker, R. Smithey, and O. Meyer, J. Phys. F: Met. Phys. **14**, L115 (1984).
[20]J. Chen, L. L. Boyer, H. Krakauer, and M. J. Mehl, Phys. Rev. B **37**, 3295 (1988).
[21]J. E. Lowther, J. Alloys Compd. **364**, 13 (2004).
[22]M. B. Kanoun, S. Goumri-Said, and M. Jaouen, Phys. Rev. B **76**, 134109 (2007).
[23]E. I. Isaev, S. I. Simak, I. A. Abrikosov, R. Ahuja, Y. K. Vekilov, M. I. Katsnelson, A. I. Lichtenstein, and B. Johansson, J. Appl. Phys. **101**, 123519 (2007).
[24]G. L. W. Hart and B. M. Klein, Phys. Rev. B **61**, 3151 (2000).
[25]A. B. Mei, O. Hellman, N. Wireklint, C. M. Schlepuetz, D. G. Sangiovanni, B. Alling, A. Rockett, L. Hultman, I. Petrov, and J. E. Greene, Phys. Rev. B **91**, 054101 (2015).
[26]Z. J. He, Z. H. Fu, D. Legut, X. H. Yu, Q. F. Zhang, V. I. Ivashchenko, S. Veprek, and R. F. Zhang, Phys. Rev. B **93**, 184104 (2016).
[27]S. Wang, X. Yu, Z. Lin, R. Zhang, D. He, J. Qin, J. Zhu, J. Han, L. Wang, H.-K. Mao *et al.*, Chem. Mater. **24**, 3023 (2012).
[28]S. Wang, H. Ge, W. Han, Y. Li, J. Zhang, X. Yu, J. Qin, Z. Quan, X. Wen, X. Li *et al.*, J. Phys. Chem. C **121**, 19451 (2017).
[29]S. Wang, H. Ge, S. Sun, J. Zhang, F. Liu, X. Wen, X. Yu, L. Wang, Y. Zhang, H. Xu *et al.*, J. Am. Chem. Soc. **137**, 4815 (2015).
[30]S. Wang, D. Antonio, X. Yu, J. Zhang, A. L. Cornelius, D. He, and Y. Zhao, Sci. Rep. **5**, 13733 (2015).
[31]S. Wang, X. Yu, J. Zhang, M. Chen, J. Zhu, L. Wang, D. He, Z. Lin, R. Zhang, K. Leinenweber *et al.*, Phys. Rev. B **86**, 064111 (2012).
[32]M. Chen, S. Wang, J. Zhang, D. He, and Y. Zhao, Chem. Eur. J. **18**, 15459 (2012).
[33]S. Wang, X. Yu, J. Zhang, L. Wang, K. Leinenweber, D. He, and Y. Zhao, Cryst. Growth Des. **16**, 351 (2016).
[34]A. Zerr, G. Miehe, J. Li, D. A. Dzivenko, V. K. Bulatov, H. Hoefer, N. Bolfan-Casanova, M. Fialin, G. Brey, T. Watanabe *et al.*, Adv. Funct. Mater. **19**, 2282 (2009).
[35]W. C. Oliver and G. M. Pharr, J. Mater. Res. **7**, 1564 (1992).
[36]G. Kresse and J. Furthmuller, Phys. Rev. B **54**, 11169 (1996).
[37]J. P. Perdew, K. Burke, and M. Ernzerhof, Phys. Rev. Lett. **77**, 3865 (1996).
[38]P. E. Blochl, Phys. Rev. B **50**, 17953 (1994).
[39]G. Hautier, S. P. Ong, A. Jain, C. J. Moore, and G. Ceder, Phys. Rev. B **85**, 155208 (2012).
[40]O. Shebanova, E. Soignard, and P. F. McMillan, High Pressure Res. **26**, 87 (2006).
[41]A. Zerr, M. Kempf, M. Schwarz, E. Kroke, M. Goken, and R. Riedel, J. Am. Ceram. Soc. **85**, 86 (2002).
[42]J. L. He, L. C. Guo, D. L. Yu, R. P. Liu, Y. J. Tian, and H. T. Wang, Appl. Phys. Lett. **85**, 5571 (2004).
[43]F. Zhou, M. Cococcioni, C. A. Marianetti, D. Morgan, and G. Ceder, Phys. Rev. B **70**, 235121 (2004).
[44]L. Wang, T. Maxisch, and G. Ceder, Phys. Rev. B **73**, 195107 (2006).
[45]V. I. Anisimov, J. Zaanen, and O. K. Andersen, Phys. Rev. B **44**, 943 (1991).
[46]L. M. Corliss, N. Elliott, and J. M. Hastings, Phys. Rev. **117**, 929 (1960).
[47]X. Dai, S. Y. Savrasov, G. Kotliar, A. Migliori, H. Ledbetter, and E. Abrahams, Science **300**, 953 (2003).
[48]S. Lutfalla, V. Shapovalov, and A. T. Bell, J. Chem. Theory Comput. **7**, 2218 (2011).
[49]S. Maintz, V. L. Deringer, A. L. Tchougreeff, and R. Dronskowski, J. Comput. Chem. **37**, 1030 (2016).
[50]R. Dronskowski and P. E. Blochl, J. Phys. Chem. **97**, 8617 (1993).
[51]A. Zunger, S. H. Wei, L. G. Ferreira, and J. E. Bernard, Phys. Rev. Lett. **65**, 353 (1990).
[52]H. J. Xiang, P. S. Wang, M. H. Whangbo, and X. G. Gong, Phys. Rev. B **88**, 054404 (2013).
[53]H. J. Xiang, E. J. Kan, S.-H. Wei, M. H. Whangbo, and X. G. Gong, Phys. Rev. B **84**, 224429 (2011).